Common-Path Dual-Comb Spectroscopy Using a Single Electro-Optic Modulator

Miguel Soriano-Amat, Marcelo A. Soto, Vicente Duran, Hugo F. Martins, Sonia Martin-Lopez, Miguel Gonzalez-Herraez, and María R. Fernández-Ruiz

***Abstract*—Dual frequency comb (DFC) spectroscopy using electro-optic comb generators stands out for its flexibility, easy implementation, and low cost. Typically, two combs with different line spacing are generated from a common laser using independent electro-optic comb generators. This approach minimizes the impact of laser phase noise; however, the distinct paths followed by the two combs ultimately limit the attainable signal-to-noise ratio and long-term stability of the system. In this work, a common-path DFC is generated using a single modulator driven by an arbitrary waveform generator, thus enabling a remarkable increase of the system stability (up to 0.8 s of integration time) while maintaining high flexibility. The proposed technique is experimentally validated by implementing a dual frequency comb with 3000 lines, covering an optical bandwidth of 4.5 GHz, and demonstrating an optical-to-radiofrequency compression factor of 7500. Our system is able to measure extremely narrowband optical features (in the MHz range) with an accuracy only limited by the master laser stability.**

***Index Terms*—Arbitrary waveform generation, brillouin scattering, dual comb spectroscopy, optical frequency combs.**

I. Introduction

OPTICAL frequency combs (OFCs) have become a groundbreaking technology in a variety of applications, such as precision spectroscopy [1], distance ranging [2] and telecommunications [3], to name just a few. In some of these applications, the interference of two OFCs with slightly different line spacing enables the acquisition of high-resolution spectra with a single photodetector and low-bandwidth electronics, thanks to an optical-to-radiofrequency (RF) down-conversion [1], [4]. Due to its seminal use for spectroscopic measurements, such a method is usually called dual-comb spectroscopy (DCS), although it can be understood in a more general way as a multi-heterodyne interferometric technique. Since their invention, dual-comb interferometers have been implemented using different comb types, including mode-locked lasers, microresonators and combs based on electro-optic (EO) or acousto-optic modulators [5]–[9]. Irrespective of the comb generation principle, resolving individual spectral lines requires the two combs involved in DCS to maintain a high degree of mutual coherence. If that condition is ensured during the acquisition time, the measurement signal-to-noise ratio (SNR) can be dramatically improved by coherent signal averaging [4], [10].

From a practical point of view, the requirement of mutual coherence between two different OFCs is technically very challenging. This condition can be accomplished, for instance, by a tight phase-locking between the combs or using digital processing algorithms. However, those methods work at the expense of increasing the hardware and/or software complexity [5], [11]. An effective approach to simplify the architecture of DCS is to use a pair of EO frequency combs generated from a single continuous-wave (CW) laser [6]–[8]. Besides its easy implementation, this scheme offers a high degree of relative phase coherence between the two combs, as well as high flexibility when setting the optical line spacing and the RF detection bandwidth. Limitations in the number of lines (typically <100) affecting the first implementations of EO combs can be overcome by external non-linear broadening [12], [13] and/or by the use of optimized electronic driving schemes [14], [15]. Using multi-stage comb generators, some EO schemes are capable of performing broadband DCS by varying the repetition rate of a single frequency comb. However, these setups require large interferometers, compromising the stability of the system and seriously limiting its capability to be reconfigured [16], [17]. Another reported strategy to produce a pair of mutually coherent OFCs is their generation from a common laser cavity [18]–[21]. In that case, the difference in the line spacing between the two combs is obtained by the asymmetries existing between the two directions of propagation inside the cavity. This architecture avoids duplicating the optical components in the setup and improves the system stability due to the common-noise rejection between the two generated combs. Several laser platforms and technologies have been employed to implement these dual-comb generators, such as bidirectional

Manuscript received November 25, 2019; revised February 12, 2020; accepted May 17, 2020. Date of publication May 28, 2020; date of current version September 15, 2020. This work was supported in part by Spanish Government (MINECO) under Projects RTI2018-097957-B-C31, RTI2018-097957-B-C32, and RTI2018-097957-B-C33, in part by Comunidad de Madrid and FEDER Program under Grant SINFOTON2-CM: P2018/NMT-4326. The work of V. Duran, H. F. Martins, and M. R. Fernández-Ruiz was supported by the Spanish MICINN under Contracts RYC-2017-23668, IJCI-2017-33856 and FJCI-2016-27881, respectively. *(Corresponding author: Miguel Soriano-Amat.)*

Miguel Soriano-Amat, Sonia Martin-Lopez, Miguel Gonzalez-Herraez, and María R. Fernández-Ruiz are with the Departamento de Electrónica, Universidad de Alcalá, Edificio Politécnico Superior, 28805 Alcalá de Henares, Spain (e-mail: miguel.soriano@uah.es; sonia.martinlo@uah.es; miguel.gonzalezh@uah.es; rosario.fernandezr@uah.es).

Marcelo A. Soto is with the Department of Electronic Engineering, Universidad Técnica Federico Santa María, 2390123 Valparaíso, Chile (e-mail: marcelo.sotoh@usm.cl).

Vicente Duran is with the GROC-UJI, Institute of New Imaging Technologies, University Jaume I, 120071 Castellón, Spain (e-mail: vduran@uji.es).

Hugo F. Martins is with the Instituto de Óptica "Daza de Valdés", IO-CSIC, 28006 Madrid, Spain (e-mail: hugo.martins@csic.es).

Color versions of one or more of the figures in this article are available online at https://ieeexplore.ieee.org.

Digital Object Identifier 10.1109/JLT.2020.2998372

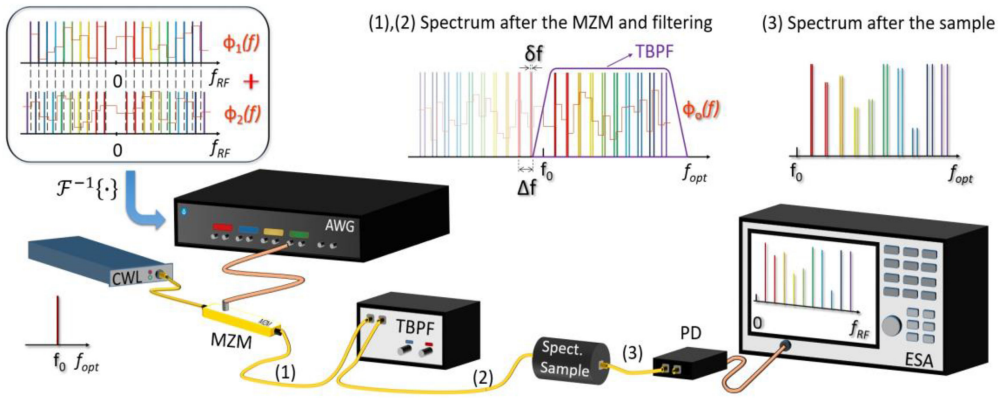

Fig. 1. (a) Conceptual scheme of the common-path dual-comb interferometer, along with the signal spectrum at different points of the scheme. Upper left inset: Detuned RF frequency combs programmed on a computer. The sketches shown here are conveniently scaled to make it evident the detuning in the line spacing and the main design features. Notice that to facilitate the optical filtering, the first line of each sideband can be separated from DC considerably more than the line spacing. CWL: continuous wave laser; AWG: arbitrary waveform generator; TBPF: optical tunable band pass filter. $F^{-1}\{\cdot\}$ stands for inverse Fourier transformation; MZM: intensity Mach-Zehnder Modulator; PD: photodetector; ESA: electrical spectrum analyzer.

mode-locked fiber lasers [18], [19], a mode-locked integrated external-cavity surface emitting laser [20] and dissipative Kerr solitons counter-propagating in a microresonator [21]. These schemes generally present limited flexibility to tune both the comb line spacing and the down-conversion factor, although some of these restrictions have been recently alleviated by the use of a bidirectional frequency-shifting loop seeded with a CW laser [22]. In all the described dual-comb schemes, the two generated frequency combs propagate along different arms before interfering, even when they are originated from the same cavity or fiber loop. In this way, thermal fluctuations or any uncorrelated noise between the two arms imposes an ultimate limit to the mutual coherence between the combs. This problem is usually circumvented by means of low-bandwidth feedback loops or phase correction algorithms [9], [23]–[25].

In this paper, we propose a method to generate a single-path dual-comb based on a single electro-optic modulator, fed by a low phase noise CW laser, and driven by an arbitrary waveform generator (AWG). The proposed scheme produces an optical spectrum composed of two interleaved frequency combs, whose line spacing differs in a small offset. This spectrum can be viewed as a sequence of periodically repeated doublets, each one composed of two lines whose frequency difference increases linearly along the optical bandwidth. The resulting dual-comb generator allows us to interrogate a spectroscopic sample with a simplified one-arm setup, which includes only one photodetector instead of a high-resolution spectrometer [1], [26]. The magnitude of the spectral fingerprinting of the sample becomes encoded onto a set of low-frequency beat notes, originated by the interference of the closest neighboring lines (doublet lines) which compose the optical dual-comb spectrum. As a proof of concept, we employ the proposed common-path dual-comb interferometer to perform a very fast measurement of the gain spectrum of stimulated Brillouin scattering (SBS) in optical fibers. The performance and limitations of the proposed method are analyzed and evaluated experimentally. Due to its common-path architecture, the implemented dual-comb interferometer allows self-referenced measurements without requiring real-time correction methods or feedback loops. The remarkable system stability achieved allows reaching integration times close to 1 second (more precisely 0.8 s) with a consistent increase in the achieved SNR across the averaged interferograms. In addition, with the current AWG technology, this method can be engineered to resolve extremely sharp optical features, in the order of MHz or below, as demonstrated hereafter.

II. Description of Comb Generator

A. Dual Comb Design and Implementation

The operation principle of our dual-comb interferometer is sketched in Fig. 1. The light source is a CW laser (NKT Koheras Basik X15) operating at $\lambda_0 = 1550.12$ nm, with a linewidth of $<$100 Hz and RIN of -135 dBc/Hz at 10 MHz. The laser light is modulated by a conventional Mach-Zehnder modulator (MZM, Photline MX-LN-10, 10 GHz). The MZM is driven by a temporal signal generated by an AWG (Keysight M8195A). This signal is previously designed off-line through the process detailed in subsection II.B The resulting digital signal includes information of both combs, whose line spacing is Δf and $\Delta f + \delta f$, respectively, being $\delta f \ll \Delta f$. This signal is then loaded into an AWG, whose electrical output is boosted by an RF amplifier and then launched into a single EO modulator. This constitutes the principal difference with conventional schemes, which add both signals in the optical domain, and are therefore subject to uncorrelated optical phase fluctuations between the combs. The MZM bias is adjusted so that the optical carrier is suppressed, therefore yielding only two symmetric sidebands around the carrier frequency [27]. Each sideband in the optical domain is a flat-top DFC. Note that the RF power entering the modulator must be as high as possible to increase the optical output power of the generated frequency combs. However, its maximum value is limited by the nonlinear behavior of the MZM. Indeed, it must be secured that the whole modulation process remains linear and free from saturation, which would otherwise produce unwanted harmonics in the spectrum. By means of a tunable optical bandpass filter (TBPF), one of the dual-comb sidebands and the residual carrier are filtered out.

Then, the light emerging from the optical filter is sent to a sample under test and detected by a single photodiode. A spectral analysis of the measured electrical signal (conveniently filtered and amplified when necessary) allows us to map line by line the optical spectrum into the electrical domain. Restricting ourselves to the lowest RF region, the interference between the nearest neighboring lines composing the dual-comb structure produces an electrical RF comb with a line spacing equal to δf. In this way, the optical bandwidth turns out to experience a compression factor (CF) calculated as $CF = \Delta f/\delta f$. Note that this downconversion is unambiguous thanks to the optical filtering performed by the TBPF, which removes the beat notes coming from the other optical sideband generated by the EO modulator. The spectral response of the spectroscopic sample becomes therefore encoded onto the dual optical frequency comb, and by spectral amplitude response of the sample can be easily retrieved. It should be noted that the electrical amplitude response encoded in the beat of each doublet corresponds to the square of the optical amplitude response of the sample, which entails double optical amplitude sensitivity compared to a setup where only one of the two combs interacts with the sample.

This configuration is similar to the symmetric or collinear approach in conventional dual-comb spectroscopy [4]. Experimentally, the reference measurement (i.e. the one without information from the sample) can be simply obtained by deviating a fraction of the light emerging from the TBPF towards a second photodiode.

B. Comb Signal Design

The design of the electrical signal driving the Mach-Zehnder modulator is carried out by a digital synthetization in the frequency domain. The process starts with the numerical construction on a computer of two single frequency combs, whose line spacing is Δf and $\Delta f + \delta f$. The frequencies that constitute the two combs are selected according to the design parameters, i.e., number of lines, optical bandwidth and frequency offset. These design parameters are subject to a series of constrains detailed in the following subsection. Defined the comb frequencies, a random phase is allocated to each spectral line in order to avoid the formation of high peak-power pulses, which can easily saturate the modulator driver and/or the photodetector. In order to recover a real-valued signal at the end of the design process (so as to obtain a real-valued electrical signal to drive the MZM), the spectrum of each comb must be conjugated symmetrically around $f = 0$ (see Fig. 1).

Once the individual combs are numerically built, they are added in the digital domain to form a single complex spectrum. Mathematically, the designed spectrum can be defined by the expression

$$E(f) = \sum_{m=0}^{N-1} A_m \left(e^{j\phi_m}\delta(f - f_m) + e^{-j\phi_m}\delta(f + f_m)\right) + \sum_{m=0}^{N-1} A_m \left(e^{j\phi_m}\delta(f - f'_m) + e^{-j\phi_m}\delta(f + f'_m)\right), \quad (1)$$

where A_m, f_m and ϕ_m are the amplitude, frequency and the random phase value of the m$^{\text{th}}$ comb line. The frequency of each line can be decomposed in terms of the line spacing

$$f_m = f_s + m\Delta f, \qquad f'_m = f'_s + m(\Delta f + \delta f), \quad (2)$$

where f_s defines the frequency of the first line of one comb ($m = 0$). The first line of the second comb (f'_s) has been set in $f'_s = f_s + \delta f$, so that, the first line of the downconverted comb can be evaluated. The time-domain representation of the modulating signal is obtained through an inverse Fourier transformation, i.e., $e(t) = IFT\{E(f)\}$. In temporal domain, $e(t)$ corresponds to a summation of cosines, each one with identical amplitude, frequency f_m and different phase value. From an implementation point of view, in this work the design of the DFCs turned out to be computationally more efficient in the spectral domain. This digital signal $e(t)$ is uploaded to the AWG to finally obtain the electrical signal driving the MZM.

C. Constraints of the Dual Comb Implementation

The basic design parameters of the DFC are the number of spectral lines *N* and the optical line spacing of each interleaved comb, given by Δf and $\Delta f + \delta f$ (with $\delta f > 0$), respectively. As it is common to all DCS setups, the need to resolve unambiguously the optical spectral lines imposes restrictions on the downconversion. Upon detection, all the optical lines of the dual comb beat to each other, in such a way that multiple bands can be found in the detected electrical spectrum. To be able to isolate the first-order beating frequencies between pairs of lines of the dual comb without aliasing, the maximum separation between pairs of lines must be smaller than half the line spacing Δf, i.e., $N\delta f < \frac{\Delta f}{2}$. When this condition is satisfied, the compressed comb can be acquired at the baseband, in the so-called first Nyquist zone (which goes from DC to $\Delta f/2$) [10]. Alternatively, we may relate δf to the optical bandwidth (BW_{opt}) as $\delta f < \frac{\Delta f^2}{2BW_{opt}}$, where $BW_{opt} = N\Delta f$. This equation has a paramount importance in dual-comb spectroscopy, since the inverse of δf corresponds to the duration of an interferogram, and therefore it defines the minimum time required to perform a complete spectroscopic measurement [4], [10].

Note that for our dual-comb generator, BW_{opt} is in principle ideally limited by the electrical bandwidth of the MZM and the AWG. Furthermore, it must be noted that the roll-off of TBPFs is typically not very sharp, leading to a further reduction of the usable bandwidth. The frequency offset δf, in its turn, depends solely on the AWG operation. In particular, the minimum value of δf is determined by the ratio between the sampling rate of the AWG to the employed memory depth (that is, by the inverse of the total time length of the generated signal). Since BW_{opt} and δf are the parameters that become fixed by the performance of the electronics and EO equipment, a downconversion without aliasing implies that $N < \sqrt{BW_{opt}/2\delta f}$. This equation reveals a tradeoff between the minimum acquisition time ($1/\delta f$) and the number of spectral lines that can be used. Once *N* is chosen, the optical line spacing is simply given by $\Delta f = BW_{opt}/N$. For the particular implementation used in this paper, BW_{opt} is

set to 4.5 GHz. Concerning the frequency offset, we employ a very narrow linewidth laser (<0.1 kHz), and a high-performance AWG featuring a sampling rate of 65 GS/s and a maximum usable memory of 320 MSa. With these specifications δf can be easily tuned over several orders of magnitude (from 200 Hz up to 100 kHz) securing hundreds or a few thousands of lines within the aforementioned optical bandwidth. Correspondingly, Δf can range from around one to a few tens of megahertz.

III. Experimental Results

A. Characterization of the Generated Dual Frequency Comb

To demonstrate the flexibility of the dual comb design and implementation, two different dual combs are presented in what follows, which have been generated employing the scheme in Fig. 1 (omitting the spectroscopic sample). The spectra of the RF signals generated by our detector (a photodiode with a bandwidth of 100 MHz) have been measured by an electrical spectrum analyzer (ESA). As mentioned above, the two dual combs are generated to cover an optical bandwidth of $BW_{opt}\sim$ 4.5 GHz. The first dual comb has N = 3000 pairs of lines, resulting in a line spacing of $\Delta f = 1.5$ MHz. The relative offset between the combs is $\delta f = 200$ Hz (i.e. the two generated combs have a line spacing of 1.5000 and 1.5002 MHz, respectively). Note that this offset corresponds to the minimum value that we can experimentally attain with our available memory depth. This configuration leads to a CF = 7500. The second DFC has N = 600 lines separated 7.5 MHz in the optical domain. In this case, the offset is set to $\delta f = 5$ kHz, what entails a CF = 1500. The obtained downconverted spectra (after photo-detection) are shown in Fig. 2. In the two cases, the ESA resolution bandwidth and video bandwidth were set in 3.3 Hz.

Fig. 2(a) shows the electrical downconverted spectrum for the DFC with 3000 line pairs. As expected, the bandwidth of the downconverted spectrum ($N\delta f$) reaches up to 600 kHz. Fig. 2(b) shows the downconverted DFC with 600 lines, and a frequency offset of 5 kHz (yielding an electrical RF spectrum of 3 MHz). With this frequency offset, it is possible to accumulate thousands of interferograms (each one with a duration of 200 μs) over acquisition times for which stabilization schemes are usually required (>0.1 s). Due to memory limitations in our oscilloscope, this was the configuration employed to analyze the evolution of the comb SNR in the time-domain, as a function of the number of averaged interferograms (see Section III.C).

An important advantage of our method is that we can optimize the form of the time-domain optical signal at the output of the comb generator, so the power per line (and thus the comb SNR) can be increased while maintaining the spectral flatness. By acting on the spectral phase of the two interleaved combs, we can avoid the generation of high peak-power sinc pulses associated to a rectangular-shaped comb with all the lines sharing (aside from a linear term) the same phase. In that "transform-limited" case, the generated sinc pulses could easily saturate the modulator driver and/or photodetector, thus imposing a significant limitation to the mean RF power required to drive the EO modulator. A full study on the optimization of the time signal released by our generator is out of the scope of this paper. However, it should

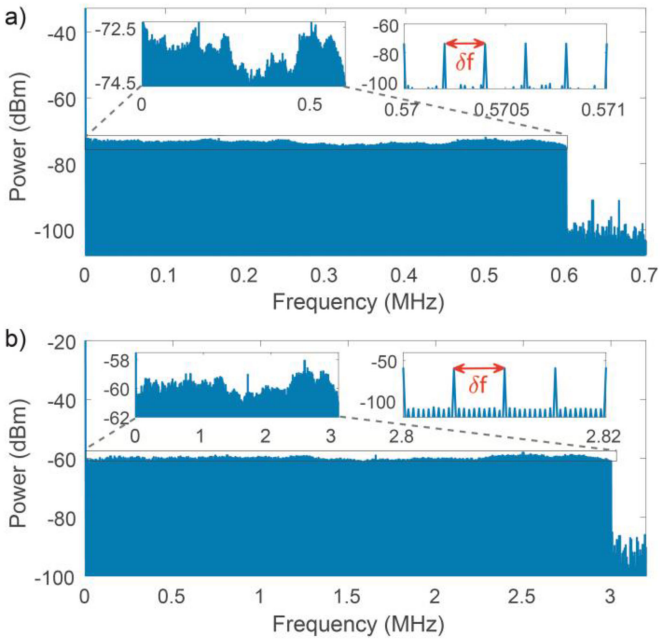

Fig. 2. Measured (downconverted) DFC spectra for: (a) N = 3000 lines, δf = 200 Hz and Δf = 1.5 MHz; (b) N = 600 lines, δf = 5 kHz and Δf = 1.5 MHz. Insets show the spectral separation of the resolved comb lines in the electrical domain (top-right) and the comb flatness in terms of electrical power (top-left).

be noted that by the simple allocation of a random phase for each spectral comb line, we experimentally verified that the average power of the combs was increased, respectively, by 19–20 dB (N = 600) and 25 dB (N = 3000) when compared to the "transform-limited" case.

B. Fine Spectral Sampling Using the Generated DFC

The features of our DFC generator allow us to produce optical frequency combs with a line spacing that can be reduced to the megahertz range. These dense combs can be exploited to perform a fine spectral sampling of narrow optical resonances by DCS [28]. The absorption lines of gases measured in conventional molecular spectroscopy have typically linewidths of a few GHz, which are too broad to benefit from the small line spacing offered by our DCS scheme. However, other spectroscopic transitions (such as those measured in saturated absorption spectroscopy [29], [30]) are a few orders of magnitude narrower and may therefore take advantage of a densified DFC.

Experimentally, we mimicked them by generating stimulated Brillouin gain and loss spectra in a conventional optical fiber, whose accurate measurement represents a challenging application to test our method. The activation of SBS requires the interaction of two counter-propagating optical signals in the fiber, which in this case are generated based on the setup depicted in Fig. 3.

The pump inserted on one side of the fiber under test (FUT) generates narrowband (a few MHz width) gain and loss processes in the fiber. In order to achieve SBS interaction, pump and probe comb have to be spectrally separated by a quantity

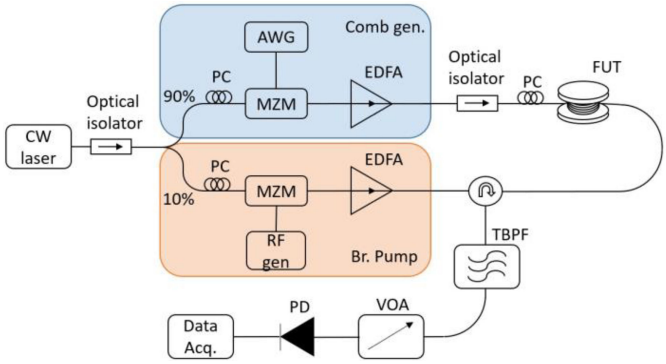

Fig. 3. Experimental setup used to demonstrate the high spectral resolution capability of the proposed common-path DFC by measuring the Brillouin gain/loss spectrum in a standard optical fiber. PC: Polarization controller. VOA: variable optical attenuator.

close to the Brillouin frequency shift (BFS) of the fiber. Using one of the DFC described in the previous section (namely, the one with N = 3000 lines), the Brillouin gain and loss spectra of a 25 km-long optical fiber have been measured. Pump power in this case is tuned to a few mW, yielding approximately 12 dB gain/loss processes in the fiber. The choice of what process is interrogated (gain or loss) is simply made depending on the relative frequency arrangement between the interacting waves (see Fig. 4-bottom, ν_B denotes the BFS of the FUT).

Experimental results recovered by the ESA are shown in Fig. 5. In particular, Figs. 5(a) and 5(c) show the down-converted electrical spectra of the comb influenced by Brillouin gain and Brillouin loss, respectively. Interestingly, the main features of the Brillouin gain/loss spectrum can be resolved with high resolution in the electrical domain, with a CF = 7500, as expected from the DFC settings.

Using this CF, the natural Brillouin gain and loss spectra are obtained in the optical domain, as shown in Fig. 5(b) and 5(d). Indeed, the Brillouin gain spectrum is measured in the electrical domain with central frequency of 351 kHz and a natural width of 4.163 kHz, representing in the optical domain a frequency offset from the master laser frequency of 8.14 GHz and a linewidth of 31.22 MHz. The Brillouin loss spectrum is measured in the electrical domain with a central frequency of 351 kHz and a natural width of 4.089 kHz. This represents in the optical domain a frequency offset from the master laser frequency of 8.14 GHz and a linewidth of 30.66 MHz. Considering the frequency offset of 19 GHz between the Brillouin pump and the master laser frequency in our setup, the measured central frequency yields a BFS of 10.86 GHz, in agreement with the value measured by conventional means [31].

C. SNR Analysis

With the purpose of evaluating the system stability, a study on the evolution of the SNR with coherent averaging is performed. In particular, the electrical SNR of the second comb characterized (N = 600 lines, δf = 5 kHz and Δf = 7.5 MHz) is computed in the time-domain, for integration times up to ≈0.8 s (corresponding to the average of 4096 interferograms, each one with a duration of 0.2 ms). The maximum number of acquired interferograms is limited in our implementation only by the memory of the employed oscilloscope. The SNR is calculated using the following strategy. Each photo-detected interferogram $s_i(t)$ is composed of the DCS signal $r(t)$ (which does not change from one interferogram to the next) and uncorrelated additive white noise $n_i(t)$:

$$s_i(t) = r(t) + n_i(t) \tag{3}$$

By using a noiseless reference interferogram, i.e., $s_{\mathrm{ref}}(t) = r(t)$, the SNR of an individual interferogram can be computed in the time domain by noting that the difference between the acquired interferogram and $s_{\mathrm{ref}}(t)$ is the noise added to the interferogram. This way, the SNR is calculated as:

$$SNR_i = \frac{\langle r(t)^2 \rangle}{\langle n_i(t)^2 \rangle} = \frac{\langle s_i(t)^2 \rangle}{\langle (s_i(t) - s_{\mathrm{ref}}(t))^2 \rangle} \tag{4}$$

where the brackets make reference to the variance calculation. In the above derivation, it has been assumed that the DFC signal of a single interferogram is strong enough so that the approximation $\langle s_i(t)^2 \rangle = \langle r(t)^2 \rangle + \langle n_i(t)^2 \rangle \approx \langle r(t)^2 \rangle$ can be used (note that the non-averaged interferograms measured by our setup present an SNR >35 dB, validating this assumption).

To compute the SNR as a function of the number of averages, we acquired in the time domain a set of 8192 interferograms employing the second configuration of our dual-comb generator. To avoid aliasing in the recorded interferograms, the first Nyquist zone is digitally filtered in the spectral domain by applying a low-pass filter to the detected signal. Note that the number of recorded interferograms in our implementation is limited by the oscilloscope memory. This dataset is then divided into two subsets of 4096 interferograms each. All the interferograms of the first subset, aligned in time, are averaged to generate a "quasi-noiseless" reference interferogram. The second subset, in its turn, is used to compute interferograms with increasing number of averages (up to 4096, which corresponds to an integration time of about 0.8 s). The evolution of SNR with the number of averages is then evaluated according to Eq. (4). Note that the "quasi-noiseless" reference interferogram and the averaged signal are disjoint sets of data, i.e., none of the interferograms used in the reference calculation were used to compute the averaged signal under analysis. Otherwise, the evaluation of the SNR would be biased. Regarding the theoretically expected value of SNR, we start by noting that for a purely additive noise, averaging *M* realizations of an interferogram should yield a reduction of the noise power by a factor of *M*:

$$\left\langle \left(\frac{1}{M} \sum_{i=1}^{M} n_i(t) \right)^2 \right\rangle = \sigma_n^2 / M \tag{5}$$

where ${\sigma_n}^2$ is the noise power of a representative trace. In this case, using a noiseless reference interferogram, averaging *M* interferograms would increase the electric SNR defined by Eq. (4) by a factor of *M*. However, in the presented implementation, the reference interferogram, while presenting very low noise, is not purely noiseless. This will affect the SNR computation as follows. Assuming a white uncorrelated noise between an

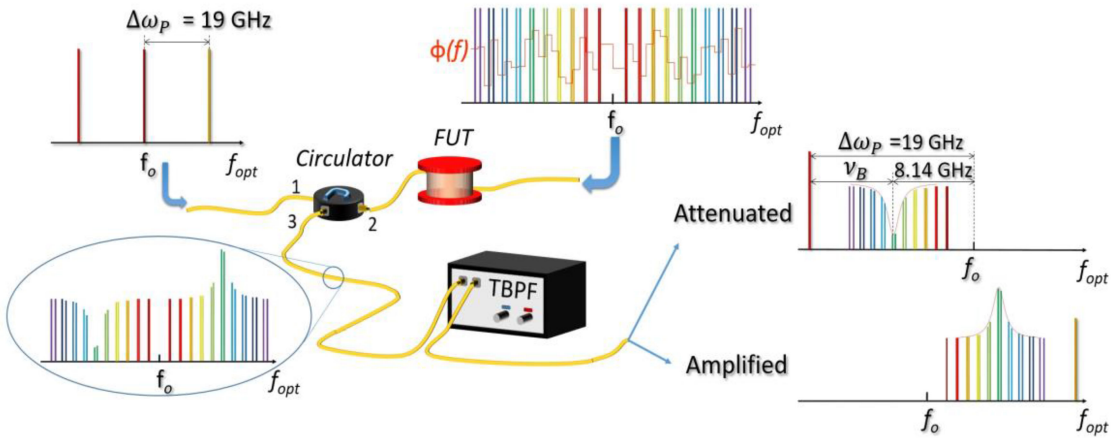

Fig. 4. Conceptual scheme of the Brillouin gain and loss processes as probed with our generated DFC.

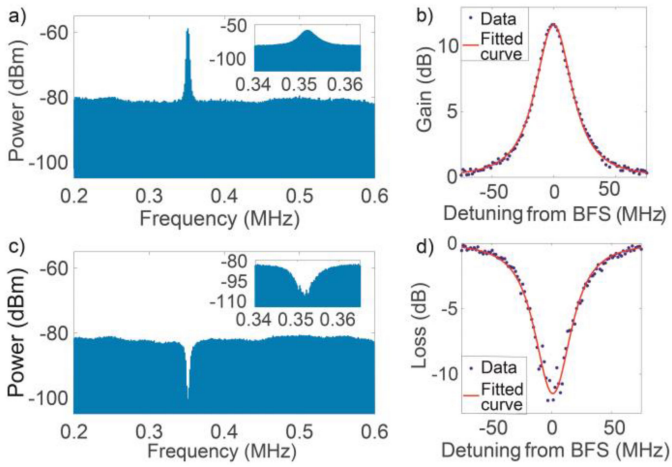

Fig. 5. DFC spectra for N = 3000 lines comb, $\delta f = 200$ Hz offset and line spacing of $\Delta f = 1.5$ MHz after interaction with the SBS gain (a) and loss (b) peaks. (c) and (d) figures show the resolved gain and loss peaks in each case, with a superimposed Lorentzian fitting. ESA resolution bandwidth and video bandwidth are both 3.3 Hz.

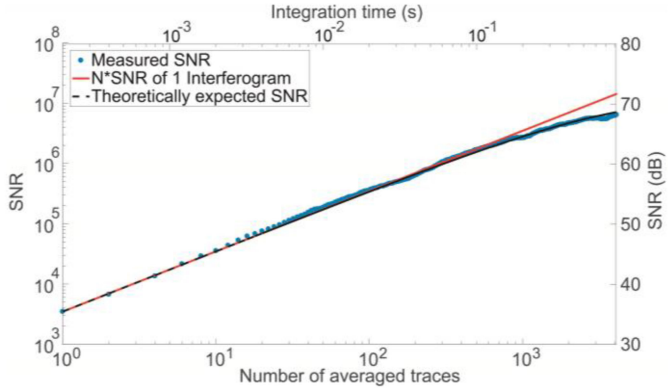

Fig. 6. Time domain electrical SNR evolution of the DFC with N = 600 lines, $\delta f = 5$ kHz and $\Delta f = 7.5$ MHz for increasing averaging times. Blue dotted line: Experimental SNR measurement. Orange solid line: additive-noise limited SNR, considering a noiseless reference. Black dashed line: additive-noise limited SNR, considering noise in the reference.

interferogram $s_i(t)$ and the reference $s_{\mathrm{ref}}(t)$ then:

$$\langle (s_i(t) - s_{\mathrm{ref}}(t))^2 \rangle = \langle n_i(t)^2 \rangle + \langle n_{\mathrm{ref}}(t)^2 \rangle \tag{6}$$

where $\langle n_{\mathrm{ref}}(t)^2 \rangle$ is the noise power in the reference interferogram, obtained with 4096 averages. Note that, for a non-averaged interferogram, the term $\langle n_{\mathrm{ref}}(t)^2 \rangle$ will be 4096 times smaller than the term $\langle n_i(t)^2 \rangle$. Then, the SNR computed for an interferogram obtained from *M* averages, will be given by:

$$SNR_{Mavg} = \frac{\left\langle \left(\frac{1}{M} \sum_{i=1}^{M} s_i(t) \right)^2 \right\rangle}{\left\langle \left(\frac{1}{M} \sum_{i=1}^{M} n_i(t) \right)^2 \right\rangle + \langle n_{\mathrm{ref}}(t)^2 \rangle} = \frac{\langle s_i(t)^2 \rangle}{\sigma_n^2 \cdot \left(\frac{1}{M} + \frac{1}{4096} \right)} = \frac{SNR_i}{\left(\frac{1}{M} + \frac{1}{4096} \right)} \tag{7}$$

In the above equation, it can be seen that for low values of *M*, the obtained SNR_{Mavg} scales, with a good approximation, proportionally to *M* (i.e. $SNR_{Mavg} \approx M \cdot SNR_i$). However, as *M* approaches 4096, the computed SNR becomes 3 dB lower than that which would be obtained with the use of a noiseless reference interferogram $s_{\mathrm{ref}}(t)$. In Fig. 6, the black dashed line presents the theoretically expected SNR computation, derived from Eq. (7) (that is, taking into account the use of a non-noiseless reference interferogram), while the orange line represents the case of a completely noiseless reference, for which $SNR_{Mavg} = M \cdot SNR_i$. The experimental results are presented in Fig. 6 in blue dotted line. Assuming infinite coherence between the frequency lines of the DFC spectrum, the electrical SNR for purely additive (white) noise is expected to increase linearly with the integration time (orange line). However, the theoretical expectation for our experimental SNR (plotted as a black dashed line in Fig. 6) needs to consider the use of a reference interferogram that is not noiseless. As can be observed, our experimental values are very close to that theoretical line. A maximum SNR of 68 dB is obtained after ≈0.8 s integration, i.e.,

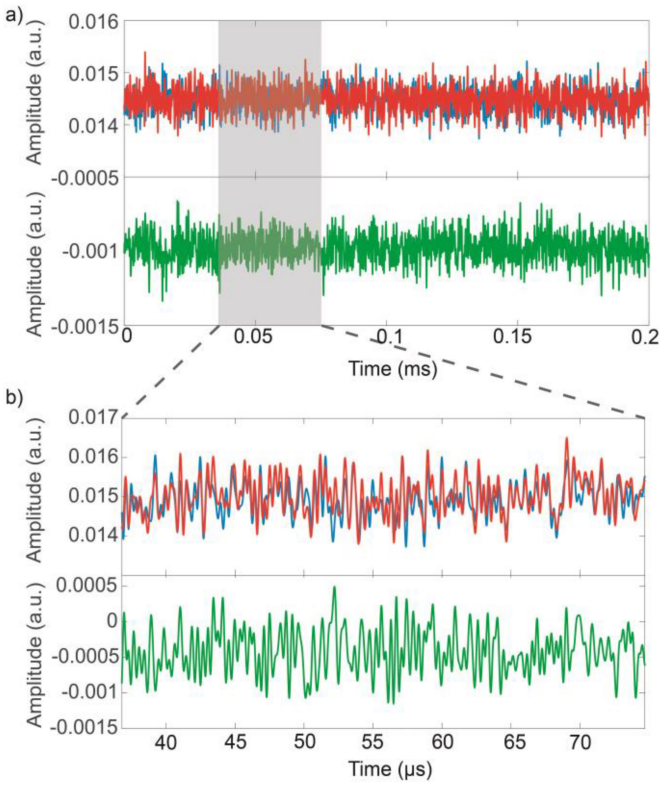

Fig. 7. (a) First (blue) and last (red) non-averaged interferograms of the dataset used to compute the SNR evolution in Fig. 6. On the bottom (green): difference between the presented interferograms. (b) Zoom-in of the curves shown in (a).

≈4000 averages. This yields an SNR improvement of 32.5 dB when compared to the SNR of a non-averaged interferogram. Note that a high stability of the system can be inferred from this figure, which indicates a continuous growth of the SNR as the number of averages increases. In case of a poor stability, the drift of the interferograms would result in lower SNR when increasing the number of averages.

A progressive saturation of the SNR starts to be noticeable only after ≈0.5 s (≈2500 averages), when the SNR is already 67.5 dB. As it is visible, this deviation is mostly explained by the use of a non-noise-free reference interferogram (black dashed line). However, the presence of non-additive noise sources at this time scale cannot be discarded. These could be related to temperature fluctuations and power drifts (from the laser or the optical amplifier, in this case an erbium doped fiber amplifier (EDFA)) or changes in the operation point of the MZM. Irrespective of the origin of the non-additive noise, the deviation from the dashed line is lower than 1dB (≈0.8 dB) at 0.8 s.

The high stability for measurements times close to 1 s is further evidenced in Fig. 7, where the first (1) and last (4096) interferograms used in the previous SNR analysis are presented. The high resemblance of the interferograms (measured with a time difference of about 1 s) can be better observed in Fig. 7(b), which shows a magnification of them. The difference between these interferograms (shown in the green line) is mostly uncorrelated (correlation coefficient <0.4) to the interferograms themselves, thus demonstrating the predominance of white noise. To reduce the impact of uncorrelated noise and better quantify the similarity of the interferograms, the correlation between the first and last 16 averaged interferograms is evaluated to be 0.975, demonstrating the high stability of the system over the time window of 1 s.

Therefore, an increase of the integration time should still yield an improvement in the attainable SNR, until the effect of power drifts and other correlated noise sources becomes more relevant. On the other hand, the effect of adding random phases to the spectral lines of the combs can also be observed in Fig. 7. The generated electrical signal is a train of noise-like waveforms that spread over the entire period (≈100% of duty cycle), thus avoiding the existence of high-peak pulses.

IV. Discussion and Conclusions

We have proposed and demonstrated the generation of a reconfigurable dual-comb spectrum using a single EO modulator driven by an AWG. This simplified scheme allows the implementation of a one-arm spectrometer capable of measuring fine spectral signatures (such as the gain spectrum of stimulated Brillouin scattering) with thousands of points and a frequency spacing of 1.5 MHz (0.01 pm). The common-path configuration of our system does not only simplify the usual EO dual-comb architecture (eliminating one arm), but also provides high stability over acquisition times of several hundreds of milliseconds. Additionally, the difference in the line spacing between the two combs, which determines the maximum measurement speed, can be tuned over three orders of magnitude (from 200 Hz to 100 kHz). The flexibility to set the different parameters of the dual-comb spectra, comparatively higher than in approaches based on bidirectional cavities, is subject, however, to several constraints and tradeoffs. The spectral coverage of our spectrometer is eventually limited by the maximum attainable modulation bandwidth. Fixed the optical bandwidth, the use of an AWG imposes a tradeoff between the number of lines and the AWG memory (Section II.B). Thus, the generation of ultra-dense frequency combs entails a large memory depth. Concerning the type of spectral information that can be measured, our common-path approach only allows us to retrieve the spectral amplitude response of a sample. In that sense, our spectrometer is analogous to (two-arm) dual-comb systems in a symmetric configuration and typical Fourier-transform infrared spectrometers.

The main limitation of the technique is currently given by the bandwidth of commercially-available electro-optic modulator, which can be of the order in 40 GHz. Unfortunately, existing methods to enlarge single EO combs cannot be used for the single-path dual-comb here generated. The reason is that those methods essentially require the two combs to propagate over different paths and/or make use of nonlinear optical effects (such as four-wave mixing), which will not be able to efficiently operate directly in the dual comb due to the non-constant spectral separation between the DFC lines. Techniques for enlarging the DFC here originated could be an interesting research topic, however this goes out of the scope of this paper.

The demonstrated dual-comb scheme explores the capability of electrical arbitrary waveform generation to engineer optical dual-comb spectra. The result is a free-running system whose

spectral region of operation can be easily extended outside the C band (to 1 μm or 2 μm) by means of the currently available EO technology. The possibility of reducing the line spacing to the megahertz level makes possible an extremely fine spectral sampling, which is of interest in applications such as spectroscopy of high-quality-factor microresonators [28], atomic spectroscopy [32] and optical sensing [14], [15], [33]. In those applications, the simple and robust design presented here represents a step towards the development of real field-deployable comb-based instruments.

Acknowledgment

MAS acknowledges AC3E Basal Project FB0008 and thanks "Becas Iberoamérica Santander Universidades Convocatoria 2018" for supporting his research stay at Universidad de Alcalá, Spain.

References

[1] N. Picqué and T. W. Hänsch, "Frequency comb spectroscopy," *Nature Photon.*, vol. 13, no. 3, pp. 146–153, Mar. 2019.
[2] I. Coddington, W. C. Swann, L. Nenadovic, and N. R. Newbury, "Rapid and precise absolute distance measurements at long range," *Nature Photon.*, vol. 3, no. 8, pp. 351–356, Jun. 2009.
[3] P. Marin-Palomo *et al.*, "Microresonator-based solitons for massively parallel coherent optical communications," *Nature*, vol. 546, no. 7657, pp. 274–279, Jun. 2017.
[4] I. Coddington, N. Newbury, and W. Swann, "Dual-comb spectroscopy," *Optica*, vol. 3, no. 4, pp. 414–426, Apr. 2016.
[5] I. Coddington, W. C. Swann, and N. R. Newbury, "Coherent multiheterodyne spectroscopy using stabilized optical frequency combs," *Phys. Rev. Lett.*, vol. 100, no. 1, pp. 013902.1–013902.4, Jan. 2008.
[6] D. A. Long *et al.*, "Multiheterodyne spectroscopy with optical frequency combs generated from a continuous-wave laser," *Opt. Lett.*, vol. 39, no. 9, pp. 2688–2690, May 2014.
[7] P. Martín-Mateos, B. Jerez, and P. Acedo, "Dual electro-optic optical frequency combs for multiheterodyne molecular dispersion spectroscopy," *Opt. Express*, vol. 23, no. 16, pp. 21149–21158, Aug. 2015.
[8] V. Durán, S. Tainta, and V. Torres-Company, "Ultrafast electro-optic dual-comb interferometry," *Opt. Express*, vol. 23, no. 23, pp. 30557–30569, Nov. 2015.
[9] V. Durán, C. Schnébelin, and H. Guillet de Chatellus, "Coherent multiheterodyne spectroscopy using acousto-optic frequency combs," *Opt. Express*, vol. 26, no. 11, pp. 13800–13809, May 2018.
[10] N. R. Newbury, I. Coddington, and W. C. Swann, "Sensitivity of coherent dual-comb spectroscopy," *Opt. Express*, vol. 18, no. 8, pp. 7929–7945, Apr. 2010.
[11] J. Roy, J.-D. Deschênes, S. Potvin, and J. Genest, "Continuous real-time correction and averaging for frequency comb interferometry," *Opt. Express*, vol. 20, no. 20, pp. 21932–21939, Sep. 2012.
[12] G. Millot *et al.*, "Frequency-agile dual-comb spectroscopy," *Nature Photon.*, vol. 10, no. 1, pp. 27–30, Jan. 2016.
[13] V. Durán, P. A. Andrekson, and V. Torres-Company, "Electro-optic dual-comb interferometry over 40 nm bandwidth," *Opt. Lett.*, vol. 41, no. 18, pp. 4190–4193, Sep. 2016.
[14] Y. Bao *et al.*, "A digitally generated ultrafine optical frequency comb for spectral measurements with 0.01-pm resolution and 0.7-μs response time," *Light Sci. Appl.*, vol. 4, no. e300, pp. 1–7, Jun. 2015.
[15] X. Yan, X. Zou, W. Pan, L. Yan, and J. Azaña, "Fully digital programmable optical frequency comb generation and application," *Opt. Lett.*, vol. 43, no. 2, pp. 283–286, Jan. 2018.
[16] M. I. Kayes and M. Rochette, "Fourier transform spectroscopy by repetition rate sweeping of a single electro-optic frequency comb," *Opt. Lett.*, vol. 43, no. 5, pp. 967–970, Mar. 2018.
[17] D. R. Carlson, D. D. Hickstein, D. C. Cole, S. A. Diddams, and S. B. Papp, "Dual-comb interferometry via repetition rate switching of a single frequency comb," *Opt. Lett.*, vol. 43, no. 15, pp. 3614–3617, Aug. 2018.
[18] S. Mehravar, R. A. Norwood, N. Peyghambarian, and K. Kieu, "Real-time dual-comb spectroscopy with a free-running bidirectionally mode-locked fiber laser," *Appl. Phys. Lett.*, vol. 108, no. 23, Jun. 2016, Art. no. 231104.
[19] X. Zhao *et al.*, "Picometer-resolution dual-comb spectroscopy with a free-running fiber laser," *Opt. Express*, vol. 24, no. 19, pp. 21833–21845, Sep. 2016.
[20] S. M. Link, D. J. H. C. Maas, D. Waldburger, and U. Keller, "Dual-comb spectroscopy of water vapor with a free-running semiconductor disk laser," *Sci.*, vol. 356, no. 6343, pp. 1164–1168, Jun. 2017.
[21] Q-F. Yang, X. Yi, K. Y. Yang, and K. Vahala, "Counter-propagating solitons in microresonators," *Nature Photon.*, vol. 11, no. 9, pp. 560–564, Sep. 2017.
[22] V. Duran, L. Djevarhidjian, and H. Guillet de Chatellus, "Bidirectional frequency-shifting loop for dual-comb spectroscopy," *Opt. Express*, vol. 44, no. 15, pp. 3789–3792, Aug. 2019.
[23] A. J. Fleisher, D. A Long, Z. D. Reed, J. T. Hodges, and F. Plusquellic, "Coherent cavity-enhanced dual-comb spectroscopy," *Opt. Express*, vol. 24, no. 10, pp. 10424–10434, May 2016.
[24] P. Guay, J. Genest, and A. J. Fleisher, "Precision spectroscopy of $H^{13}CN$ using a free-running, all-fiber dual electro-optic frequency comb system," *Opt. Lett.*, vol. 43, no. 6, pp. 1407–1410, Mar. 2018.
[25] P. Martín-Mateos, B. Jerez, P. Largo-Izquierdo, and P. Acedo, "Frequency accurate coherent electro-optic dual-comb spectroscopy in real-time," *Opt. Express*, vol. 26, no. 8, pp. 9700–9713, Apr. 2018.
[26] S. A. Diddams, L. Hollberg, and V. Mbele, "Molecular fingerprinting with the resolved modes of a femtosecond laser frequency comb," *Nature*, vol. 445, no. 7128, pp. 627–630, Feb. 2007.
[27] M. R. Fernández-Ruiz, M. Li, and J. Azaña, "Time-domain holograms for generation and processing of temporal complex information by intensity-only modulation processes," *Opt. Express*, vol. 21, no. 25, pp. 10314–10323, Apr. 2013.
[28] N. B. Hébert, V. Michaud-Belleau, S. Magnan-Saucier, J.-D. Deschênes, and J. Genest, "Dual-comb spectroscopy with a phase-modulated probe comb for sub-MHz spectral sampling," *Opt. Lett.*, vol. 41, no. 10, pp. 2282–2285, May 2016.
[29] D. W. Preston, Doppler-free saturated absorption: Laser spectroscopy" *Amer. J. Phys.*, vol. 64, no. 11, pp. 1432–1436, Nov. 1996.
[30] I. S. S. T. Hänsch and A. L. Schawlow, "High resolution Saturation Spectroscopy of the Sodium D lines with a pulsed tunable dye laser," *Phys. Rev. Lett.*, vol. 27, no. 11, pp. 707–710, Sep. 1971.
[31] M. Nikles, L. Thevenaz, and P. A. Robert, "Brillouin gain spectrum characterization in single-mode optical fibers," *J. Lightw. Technol.*, vol. 15, no. 10, pp. 1842–1851, Oct. 1997.
[32] D. A. Long, A. J. Fleisher, D. F. Plusquellic, and J. T. Hodges, "Multiplexed sub-doppler spectroscopy with an optical frequency comb," *Phys. Rev. A.*, vol. 94, no. 6, pp. 061801.1–061801.7, Dec. 2016.
[33] J. Posada-Roman, J. A. Garcia-Souto, D. A. Poiana, and P. Acebedo, "Fast interrogation of fiber bragg gratings with electro-optical dual optical frequency combs," *Sensors*, vol. 16, no. 12, pp. 2007.1–2007.11, Nov. 2016.

Miguel Soriano-Amat received the bachelor's degree in physics and the master's degrees in advanced physics from the Universitat de València, Valencia, Spain, in 2017 and 2018, respectively. He is currently a Doctoral Researcher with the Photonics Engineering Group, University of Alcalá, Alcalá de Henares, Spain. His research activities are focused on the developing of novel complex modulation techniques for distributed acoustic sensing systems.

Marcelo A. Soto received the M.Sc. degree in electronic engineering from Universidad Técnica Federico Santa María, Valparaíso, Chile, in 2005, and the Ph.D. degree in telecommunications from the Scuola Superiore Sant Anna, Pisa, Italy, in 2011. During 2010–2011, he was a Research Fellow with Scuola Sant'Anna, where he worked on distributed optical fiber sensors based on Raman and Brillouin scattering. Later, he was a Postdoctoral Researcher with the EPFL Swiss Federal Institute of Technology of Lausanne, Switzerland, where he worked on high-performance Brillouin and Rayleigh distributed fiber sensing, nonlinear fiber optics, optical signal processing, and optical Nyquist pulse generation. Since March 2018, he has been a Tenure-Track Assistant Professor with Universidad Técnica Federico Santa María, Valparaíso, Chile. He also has an invited position as one of the "100 distinguished invited professors" with Guangzhou University, China. He is the author or coauthor of more than 170 scientific publications in international refereed journals and conferences, three book chapters, and eight patents in the fields of optical communications and optical fiber sensing. He is a member of the Optical Society of America, and is in the Board of Reviewers of major international journals in photonics.

Vicente Duran received the Ph.D. degree in physics from Universitat de Valencia, Valencia, Spain, in October 2007. He has been working on a wide range of areas and relevant technologies in Photonics: spatial light modulators, adaptive optics, multidimensional imaging, compressive sensing, imaging in scattering media, and optical frequency combs. His research career has been carried out in several European research institutions, namely Universitat Jaume I, Spain, Chalmers University of Technology, Sweden, and Université Grenoble-Alpes, France. In 2014, he was awarded a Marie Curie fellowship (Excellence Science pillar of the EU Framework Programme). From 2019, he has been a Postdoctoral Researcher with Universitat Jaume I within the programme Ramón y Cajal of the Spanish State Research Agency. His records include 30 papers in indexed journals, more than 75 contributions to conferences (more than 10 invited talks), and three book chapters edited by CRC Press, Wiley, and Springer-Verlag. His work has received more than 1100 citations (Scopus). He has also participated in a number of competitive research projects (national and EU-funded) and is currently the Principal Investigator in one national project.

Hugo F. Martins received the Ph.D. degree in physics under jointly-awarded Ph.D. program with the University of Porto, Porto, Portugal and the University of Alcala, Madrid, Spain, in 2014. The topic of the doctoral dissertation was the use of Raman effect to assist distributed and remote fiber sensing. His research career has been mainly focused on distributed optical fiber sensing, mainly the use of phase-sensitive optical time domain reflectometry for distributed vibration/intrusions and temperature/strain detection along large structures/perimeters, with recent focus on the use of chirped-pulse phase-sensitive OTDR. He is currently part of the research staff of the University of Alcalá, Alcalá de Henares, Spain. He is the author or coauthor of more than 50 papers in international refereed journals and international conference contributions, with more than 500 citations, coauthor in three patents and participated in more than 10 R&D projects (both in research and industry). He has received several important scientific recognitions, including the award of best Ph.D. Thesis in Optics and Photonics of 2014 in Portugal by the "Sociedade Portuguesa de Óptica e Fotónica" (Portuguese Society of Optics and Photonics).

Sonia Martin-Lopez received the Ph.D. degree from the Universidad Complutense de Madrid, Madrid, Spain, in May 2006. The topic of her doctoral dissertation was on experimental and theoretical understanding of continuous-wave pumped supercontinuum generation in optical fibers. She had a Predoctoral stay with the Nanophotonics and Metrology Laboratory, Ecole Polytechnique Federale de Lausanne, Lausanne, Switzerland. She has been involved as a Postdoctoral Researcher with the Applied Physics Institute and with the Optics Institute, Spanish Council for Research for six years. She is currently an Associate Professor with the Photonics Engineering Group, University of Alcalá, Alcalá de Henares, Spain. She is the author or coauthor of more than 200 papers in international refereed journals and conference contributions. Her current research interests include nonlinear fiber optics and distributed optical fiber sensors.

Miguel Gonzalez-Herraez received the D.Eng. degree in telecommunications engineering from Universidad Politécnica de Madrid, Madrid, Spain, in 2004. Since 2004, he has been with the Department of Electronics, University of Alcalá, Alcalá de Henares, Spain, where he is currently a Full Professor. His current research interests include distributed optical fiber sensing, nonlinear fiber optics, and ultrafast fiber lasers. He is the author or coauthor of more than 120 research articles in indexed journals and more than 140 contributions to prestigious international conferences in the field of photonics, more than 15 of them invited or plenary. He is the coauthor of eight patents, three of which are being exploited by companies in the domain. His works have received more than 4200 citations. He has also been the Principal Investigator in a number of competitive research projects (national and EU-funded) and several research contracts financed by companies. He is referee of all journals related to photonics as well as many research funding agencies. Along in his career, he has received significant recognitions to his research work. In particular, in 2012, he was recognized with a prestigious ERC Starting Grant awarded by the European Research Council (ERC) and endowed with approximately 1.5 M €. He has also received the "Agustín de Betancourt y Molina Award," given by the Spanish Royal Academy of Engineering and the "Miguel Catalán" Award granted by the Government of Madrid. He is an Associate Editor for the *IEEE Photonics Technology Letters*, and a Senior Member of the Optical Society of America.

María R. Fernández-Ruiz received the B.Eng. degree in telecommunications and the M.Eng. degree in electronic systems and signal processing from the University of Seville, Seville, Spain, in 2009 and 2011, respectively, and the Ph.D. degree in telecommunications from the University of Quebec, Quebec City, QC, Canada, in 2016. During this period, she worked on advanced photonic signal processing techniques inspired by the space-time duality for ultrafast optical signals, and new ultra-broadband optical processors based on fiber Bragg gratings. She is currently a Postdoctoral Research Fellow with the Photonics Engineering Group, University of Alcalá, Alcalá de Henares, Spain. Her research activities focus on the development of novel techniques for enhancing the performance (resolution, range) of distributed acoustic sensor systems. She is the author or coauthor of more than 65 papers in international refereed journals and conference contributions. Her current research interests include optical signal processors, nonlinear optics, and distributed optical sensors.